Journal of Sound and Vibration 473 (2020) 115243

Contents lists available at ScienceDirect

Journal of Sound and Vibration

journal homepage: www.elsevier.com/locate/jsvi

Design, construction and experimental performance of a nonlinear energy sink in mitigating multi-modal vibrations

Kevin Dekemele [a,*], Patrick Van Torre [b], Mia Loccufier [a]

[a] Ghent University, Department of Electromechanical, Systems and Metal Engineering, Tech Lane Ghent Science Park, Campus A 125, 9052, Ghent, Belgium

[b] Ghent University, Department of Information Technology, Tech Lane Ghent Science Park, Campus A 126, 9052, Ghent, Belgium

ARTICLE INFO

Article history:
Received 2 October 2019
Revised 20 January 2020
Accepted 9 February 2020
Available online 10 February 2020
Handling Editor: P Tiso

Keywords:
Nonlinear energy sink
Mechanical design
Targeted energy transfer
Resonance capture cascade

ABSTRACT

To passively reduce the vibration energy in mechanical systems under shock load, nonlinear energy sinks (NES) can be locally attached, serving as vibration absorbers. The NES is an alternative to the standard tuned-mass-damper (TMD). While the TMD has a linear connecting spring, the NES has a nonlinear one. As a consequence, the NES has an energy dependent natural frequency. Because of this property, the NES is able to mitigate multi-modal transient vibrations sequentially from high to low frequency through a resonance capture cascade (RCC). This is a major advantage over the TMD, which is tuned only to reduce vibrations in a narrow frequency band, typically a single mode. Recently, three performance measures for the NES were derived, 1) The energy dissipation, the amount of total vibration energy dissipated by the NES. 2) The pumping time that estimates the time required for the NES to absorb a single frequency and 3) the cascading time, estimating the time the NES engages in RCC, absorbing all the modal frequencies. The novelty of these measures is that they only require the knowledge of the system's parameters. In this research, a complete implementation of a NES is presented, from design and practical realization, to verifying the performance measures experimentally. The performance measures thus allow to predict experimental performance of the NES without simulations or experiments, opposite to what literature does. The NES is constructed with a novel design methodology. This methodology allows for tailor made purely nonlinear stiffness. The NES is placed on a frame representing a scale model single-story building, to validate the single-mode performance. To obtain resonance cascading, a second story is added to obtain a two-mode dominant vibrating structure. The cascading time is predicted and confirmed by the experiments. The experiments agree well with both simulations and predictions regarding performance. This work validates the ease of use of the performance measures and their ability to predict experimental performance of a NES mitigating multi-modal vibrations.

* Corresponding author.
E-mail address: kevin.dekemele@ugent.be (K. Dekemele).

https://doi.org/10.1016/j.jsv.2020.115243
0022-460X/

1. Introduction

To passively mitigate vibration energy in mechanical systems, tuned-mass-dampers (TMD) are locally connected to system. A TMD is a linear mass-spring-damper system with a single natural frequency. TMDs are tuned in such a way that their natural frequency is close to a single vibration mode of the mechanical system. The TMD will capture this tuned mode, while it will fail to reduce the vibration energy of other vibration modes. To increase the frequency band of vibration mitigation, nonlinear energy sinks (NES) have been proposed. A NES is connected to the mechanical system through a nonlinear stiffness [1]. Because of the nonlinearity, there is no fixed natural frequency, and in a free vibration the NES can vibrate with virtually any frequency, depending on the initial energy. Inherent to the NES, is that vibration energy has to be above an energy threshold to significantly reduce vibrations. If a mechanical system is impulsivly loaded above the energy threshold, the NES will engage in so-called targeted energy transfer (TET), where the vibration energy is transferred to the NES, where it is dissipated. The TET mechanism is characterized by a finite duration of the mitigation (called pumping time) and a residual amount of vibration energy after TET, which is reduced very slowly. This is in sharp contrast to the linear TMD, which dissipates the energy exponentially (forever) to zero. The finite duration and residual energy was discussed previously [2], but has been given significant attention in a previous work by the author of the current work [3] for NESs with polynomial stiffness. There, it was investigated which parameters could expedite this duration and decrease the residual energy. Both the residual energy and pumping time in Ref. [3] could be calculated from the mechanical system's and NES's parameters. As a consequence, the NES performance could be assessed without the need of extensive simulations, contrary to what is typically done to asses the NES performance [1,4,5].

As a consequence of the NES's variable natural frequency it can mitigate vibrations of different frequencies. If attached to a multi-modal vibrating system, the NES will engage in TET for each mode separately and sequentially, from high to low frequency. This phenomenon is called resonance capture cascade (RCC). This unique feature was given some attention over a decade ago [6–8], but faded into the background. In Ref. [3], it was shown that the duration of resonance cascading is made up of the individual pumping times of each contributing mode. This cascading time could be also predicted from solely the system's parameters.

In this paper, the performance measures will be used to predict the NES performance in an experimental setup.

TET was first experimentally verified in Ref. [9]. The NES was realized by clamping a thin steel wire having a lumped mass in the middle representing the NES mass. When subjected to transversal forces, the restoring force, when approximated by a Taylor series, has a cubic nonlinearity. This NES realization was further used in other works [7,10,11]. The coefficient of nonlinearity could be altered by adjusting the length of the clamped wire. Difficulties in clamping and snapping of the wire led others to replace the steel wire by linear springs [12–14] while retaining the transverse vibrations.

In Ref. [15], pyramid-shaped elastomeric bumpers were used to approximately obtain a cubic stiffness relation. The coefficient is determined by the geometry of the bumper. A novel design was proposed in Ref. [16], consisting of parallel leaf springs approximating a cubic stiffness force with a piecewise linear restoring force. To adjust the spring characteristic, a new assembly of leaf springs has to be built. In Ref. [17], a NES was proposed and built, consisting of a magnet translating in a repulsive magnetic field provided by other magnets. Its characteristic, that could be adjusted by swapping out magnets, consisted of a combination of linear, cubic and quintic nonlinearities. This magnetic NES was subsequently tested on a multi-story structure in Ref. [18]. Another design was proposed in Ref. [19], where a linear spring is constrained to a nonlinear track on one end and fixed on the other end is. The spring is allowed to move in both the lateral and axial direction. The resulting characteristic was an asymmetric irrational function. All of the NES realizations mentioned above either only approximate the cubic nonlinearity or have difficult to adjust nonlinear coefficient which often requires manufacturing another NES. Therefore, a different design will be proposed and implemented here.

In the aforementioned experimental investigations, the NES is often placed on a system that mainly vibrate according to a single dominant mode. Also, the performance of the NES could only be assessed after extensive simulations or experiments. The experimental works in Ref. [7] do showcase RCC, but there was no attempt to classify the performance of the NES during RCC. In the current paper, the NES will be attached to a mechanical system having two dominant modes.

The aim of this research is to simplify the experimental implementation of a NES in mitigating transient multi-modal vibrations, from design to prediction and quantifying performance. The main contributions are: 1) Proposing a novel NES design, that inherently has a purely cubic stiffness and with complete control of the coefficient. 2) Showing the ability of the performance measures (pumping time, energy dissipation and cascading time) in predicting the experimental NES performance. This solely from the NES and mechanical system parameters as opposed to extensive simulation or experiments. 3) Focusing on the experimental performance of resonance capture cascading. Previous experimental works either focussed on single mode TET or only briefly discussed the RCC capabilities of their experimental setups.

This research is structured as follows: In section 2, the novel NES design methodology is proposed and the final engineered NES is shown. In the 3rd section the theoretical dynamics of the main system and NES are derived and the 3 performance measures are defined, i.e. pumping time, residual energy and cascading time. In section 4 the parameters of the engineered NES are identified with the restoring force surface method [20,21]. The two frames that serve as the main system are also identified as an equivalent mass-spring-damper system. With the system parameters available, the performance of the NES in mitigating vibrations for both the single and double frame mechanical system can be predicted with the performance measures. Finally, the NES performance is finally experimentally verified in section 5, both in the uni- and multimodal case, proving the simplicity and utility of the performance measures in experimental applications.

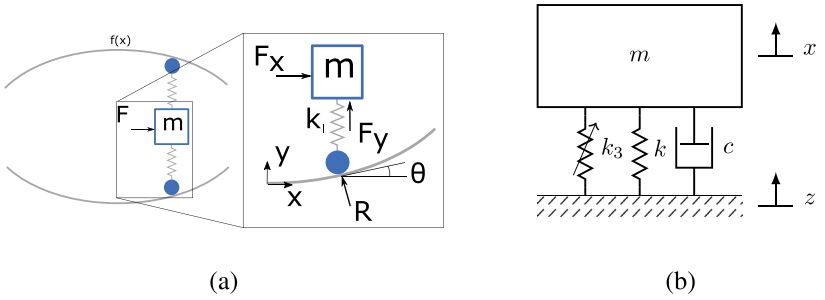

(a) (b)

Fig. 1. Design principle of the NES (a) and equivalent dynamical model (b).

2. Design of a nonlinear energy sink

2.1. Design principle

A mass-spring mechanism is depicted in Fig. 1a. The mass is constrained to move in the x direction. To both linear springs k_l a follower is attached. As the mass moves in the x direction, the followers move along a nonlinear track, a force profile $f(x)$, which compresses the springs axially. If a static force F_x is applied to the mass, moving it over a distance x, the mass will push back with an equivalent stiffness force. The linear springs are compressed with y by the force profile and exert a force on the mass in the y direction, $F_y = k_l f(x)$. By attaching springs to each side of the mass, the total force on the mass is cancelled in the y-direction. The force profile exerts a reaction force R on the followers. In the design, we have control over the force profile $f(x)$ and the linear springs k_l. Now, a relation is sought between the equivalent spring force F_x and the design parameters k_l and $f(x)$.

The x and y forces are related to the follower reaction force as follows:

$$F_x = 2R\sin(\theta) \quad F_y = R\cos(\theta) \Rightarrow F_x = 2F_y\tan(\theta) \tag{1}$$

with θ the slope angle of $f(x)$, related to the force profile by $\tan\theta = \frac{df(x)}{dx}$. If $f(x) = ax^2 + b$, F_x, which represents the nonlinear stiffness characteristic, becomes:

$$F_x = 2k_l f(x)\frac{df(x)}{dx} = 4k_l a(bx + ax^3) = kx + k_3x^3 \tag{2}$$

with $k = 4k_l ab$ and $k_3 = 4k_l a^2$.

By precisely machining the force profile, the nonlinear stiffness of the NES can be tailor made. For a given force profile, k_3 can also be tuned with the linear springs k_l. The linear coefficient of (2) can be adjusted by simply shifting a manufactured profile $f(x) = ax^2$ over a distance b, pre-stressing the linear springs k_l. In the experiments there is no pre-tension so $k = 0$. The equivalent model is given in Fig. 1b, with the addition of damping.

Unique to the presented design is the control over the coefficients k and k_3, and the ability of achieving a purely cubic NES. The ensured exact stiffness design allows to predict the performance using the performance measures defined in Ref. [3].

2.2. Practical realization

A mass of 0.49 kg is put on the sled of a linear guide rail. This rail constrains the movement of the mass to a single direction. The force profile $f(x)$ was machined by a CNC mill with $a = 4\ \mathrm{m}^{-1}$. As followers, rolling bearings were selected. The linear springs are reported by the manufacturer to have a stiffness of $k_l = 16.7$ kN. The cubic stiffness according to (2) is then $k_3 = 1.07\ \mathrm{MN\,m}^{-3}$. The realization of the NES is shown in Fig. 2a. The NES is placed on a shaking table in Fig. 2b. If the shaking table imposes a base motion of $z(t)$, the dynamical behavior is described in the following nonlinear differential equation:

$$m_{na}\ddot{x} = -c(\dot{x} - \dot{z}) - k(x - z) - k_3(x - z)^3 \tag{3}$$

with m_{na} the NES mass and c the equivalent damping, introduced by the practical realization in the guide and followers. In Section 4, the spring characteristic will be identified.

3. Mechanical system and NES dynamics and performance

3.1. Governing equations

The considered vibrating system is modeled as a multi-degree-of-freedom (MDOF) lumped mass-spring-damper system with $x \in \mathbb{R}^{n\times 1}$ the physical degrees of freedom.

$$\mathbf{M}\ddot{\mathbf{x}}(t) + \mathbf{C}\dot{\mathbf{x}}(t) + \mathbf{K}\mathbf{x}(t) = 0 \tag{4}$$

Fig. 2. Realization of NES design (a) on shacking table (b).

with $\mathbf{M} \in \mathbb{R}^{n\times n}$ the mass matrix, $\mathbf{C} \in \mathbb{R}^{n\times n}$ the viscous damping matrix, $\mathbf{K} \in \mathbb{R}^{n\times n}$ the stiffness matrix. The eigenvalue problem yields n eigenfrequencies ω_i and the eigenvector matrix, $\mathbf{E} = [\mathbf{e_1} \quad \mathbf{e_2} \quad \dots \quad \mathbf{e_n}] \in \mathbb{R}^{n\times n}$. These allow for modal decomposition $\mathbf{x} = \mathbf{Eq}$, $\mathbf{q} \in \mathbb{R}^{n\times 1}$. Then, by attaching the NES to coordinate x_ℓ, the dynamics of the compound system in modal coordinates are:

$$\begin{cases} \mathbf{M}_q\ddot{\mathbf{q}} + \mathbf{C}_q\dot{\mathbf{q}} + \mathbf{K}_q\mathbf{q} + \mathbf{e}^T_{*(\ell)}(c_{na}(\dot{x}_\ell - \dot{x}_{na}) + k_{na}(x_\ell - x_{na})^3 + k_{lin}(x_\ell - x_{na})) = 0 \\ m_{na}\ddot{x}_{na} + c_{na}(\dot{x}_{na} - \dot{x}_\ell) + k_{na}(x_{na} - x_\ell)^3 + k_{lin}(x_{na} - x_\ell) = 0 \end{cases} \tag{5}$$

with $e_*(\ell) \in \mathbb{R}^{n\times 1}$ the ℓ-th row of $\mathbf{E}$, $\mathbf{M}_q = \mathbf{E}^T\mathbf{ME}$ the modal mass matrix, $\mathbf{C}_q = \mathbf{E}^T\mathbf{CE}$ the modal damping matrix, and $\mathbf{K}_q = \mathbf{E}^T\mathbf{KE}$ the modal stiffness matrix. The forces exerted by the NES on the mechanical system can be replaced by its inertia:

$$\begin{cases} \mathbf{M}_q\ddot{\mathbf{q}} + \mathbf{C}_q\dot{\mathbf{q}} + \mathbf{K}_q\mathbf{q} + \mathbf{e}^T_{*(\ell)}m_{na}\ddot{x}_{na} = 0 \\ m_{na}\ddot{x}_{na} + c_{na}(\dot{x}_{na} - \dot{x}_\ell) + k_{na}(x_{na} - x_\ell)^3 + k_{lin}(x_{na} - x_\ell) = 0 \end{cases} \tag{6}$$

To simplify the analysis, it is assumed that the system vibrates with a single vibration mode i: $\mathbf{x}(\mathbf{t}) = \sum_{k=1}^{n} \mathbf{e_k}q_k(t) = \mathbf{e_i}q_i(t)$. The assumption is fair, as during the resonance cascade the NES interacts with a single frequency at a given time. The NES attachment point $x_\ell = e_i(\ell)q_i$ is reintroduced:

$$\begin{cases} \ddot{x}_\ell + \varepsilon\lambda\dot{x}_\ell + \omega_i^2 x_\ell + \varepsilon\ddot{x}_{na} = 0 \\ \varepsilon\ddot{x}_{na} + \varepsilon\lambda_{na}(\dot{x}_{na} - \dot{x}_\ell) + \varepsilon\Omega_3\omega_i^4(x_{na} - x_\ell)^3 + \varepsilon\kappa\omega_i^2(x_{na} - x_\ell) = 0 \end{cases} \tag{7}$$

with

$$\varepsilon\lambda = \frac{c_{q,i}}{m_{q,i}} \quad \omega_i^2 = \frac{k_{q,i}}{m_{q,i}} \quad \varepsilon = \frac{m_{na}e_i^2(\ell)}{m_{q,i}} \quad \kappa = \frac{k_{lin}}{m_{na}\omega_i^2} \quad \lambda_{na} = \frac{c_{na}}{m_{na}} \quad \Omega_3 = \frac{k_{na}}{m_{na}\omega_i^4}$$

The mass ratio is assumed $\varepsilon \ll 1$, implying that the coefficient of each NES term in (6) is small. The $n+1$ DOF problem is reduced to a 2DOF problem, because of the single mode assumption, depicted in Fig. 3. For the single mode assumption to hold, both ε and κ should remain small to have a weak coupling between NES and the mechanical system. The differential equation in (7) does not allow an exact analytic solution because of the nonlinearities. Therefore, semi-analytic techniques are applied next to yield an approximate solution.

3.2. Slow flow dynamics

The nonlinear differential equation is simplified by consecutively applying the following steps:

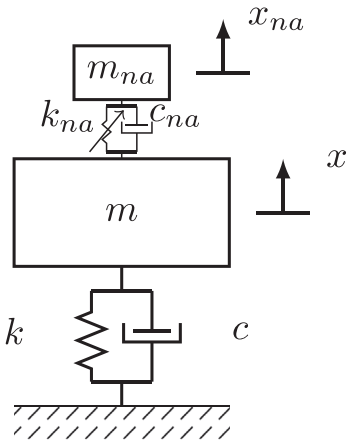

Fig. 3. The equivalent 2DOF oscillator obtained from the single-mode vibrating assumption of the mechanical system.

- Complexification of x and x_{na} to $\phi(t)e^{j\omega_i t} = \dot{u} + j\omega_i u$ and $\phi_{na}(t)e^{j\omega_i t} = \dot{v} + j\omega_i v$, ϕ_{na} and $\phi \in \mathbb{C}$, with $u = x_\ell + \varepsilon x_{na}$ the center of mass of the compound system and $v = x_{na} - x_\ell$ the relative absorber coordinate.
- Expressing the complex variables ϕ and ϕ_{na} in a perturbation series in function of ε; $\phi = \phi_0 + \varepsilon\phi_1$ and $\phi_{na} = \phi_{na,0} + \varepsilon\phi_{na,1}$
- Decomposing the dynamics on two time scales $T_0 = t$, the fast time, and $T_1 = \varepsilon t$, the slow time, an subsequently express the dynamics only in T_1, $\phi_0(T_1)$ and $\phi_{na,0}(T_1)$.
- Rewriting the complex slow time variables into the polar notation $\phi_0(T_1) = R_0 e^{j\delta_0}$ and $\phi_{na,0}(T_1) = R_{na}e^{j\delta_{na}}$.
- Introducing the dimensionless energy variables $Z_0 = \Omega_3 E_0$ and $Z_{na} = \Omega_3 E_{na}$, with $E_0 = R_0^2 = |\phi_0(T_1)|$ and $E_{na} = R_{na}^2 = |\phi_{na}(T_1)|$.
- Damping is made dimensionless with $\xi = \frac{\lambda}{\omega_i}$ and $\xi_{na} = \frac{\lambda_{na}}{\omega_i}$

For the complete derivations, please refer to Ref. [3]. The result is the slow flow dynamics of Z_0 and Z_{na}:

$$\begin{aligned} \frac{\partial Z_0}{\partial T_1} &= -\lambda Z_0 - \lambda_{na} Z_{na} \\ Z_0 &= \left[\xi_{na}^2 + \left(1 - \kappa - \frac{3}{4}Z_{na}\right)^2\right] Z_{na} \end{aligned} \tag{8}$$

Equation (8) describe the dynamics of the vibration energy on a slow time scale. The first equation states that Z_0 always decreases. The second is a static relation between Z_{na} and Z_0, that is the slow invariant manifold (SIM) on that confines the relation between Z_{na} and Z_0. A collection of SIMs are shown in Fig. 4a and b. The SIM has two extrema as long as $\xi_{na} < \frac{(1-\kappa)}{\sqrt{3}}$:

$$\begin{cases} Z_{na\pm} = \dfrac{4}{9}\left(2(1-\kappa) \pm \sqrt{(1-\kappa)^2 - 3\xi_{na}^2}\right) \\ Z_0^{\pm} = \left[\xi_{na}^2 + \left(1 - \kappa - \dfrac{3}{4}Z_{na}^{\mp}\right)^2\right] Z_{\mp}^{na} \end{cases} \tag{9}$$

With the existence of these extrema, there are 3 branches in the interval $[Z_0^-, Z_0^+]$.

3.3. Tuning NES with SIM

The efficiency of the NES depends on where the dynamics initiate on the SIM. When the dynamics initiate on the right branch ($Z_0 > Z_0^-$ and $Z_{na} > Z_{na}^+$), Z_{na} is large and therefore $\frac{\partial Z_0}{\partial T_1}$ is large and negative, (8). This fast decrease of Z_0 is TET. The right branch is descended by the dynamics until $\{Z_{na}^+, Z_0^-\}$, see Fig. 4c. As $\frac{\partial Z_0}{\partial T_1}$ is always negative, the dynamics can not ascend the SIM at any point. Rather, the dynamics will jump to the left branch. Here, Z_{na} is small, so $\frac{\partial Z_0}{\partial T_1}$ is small as well, with the residual vibration energy Z_0^- only gradually decreasing. The middle branch was shown to be unstable [2,22].

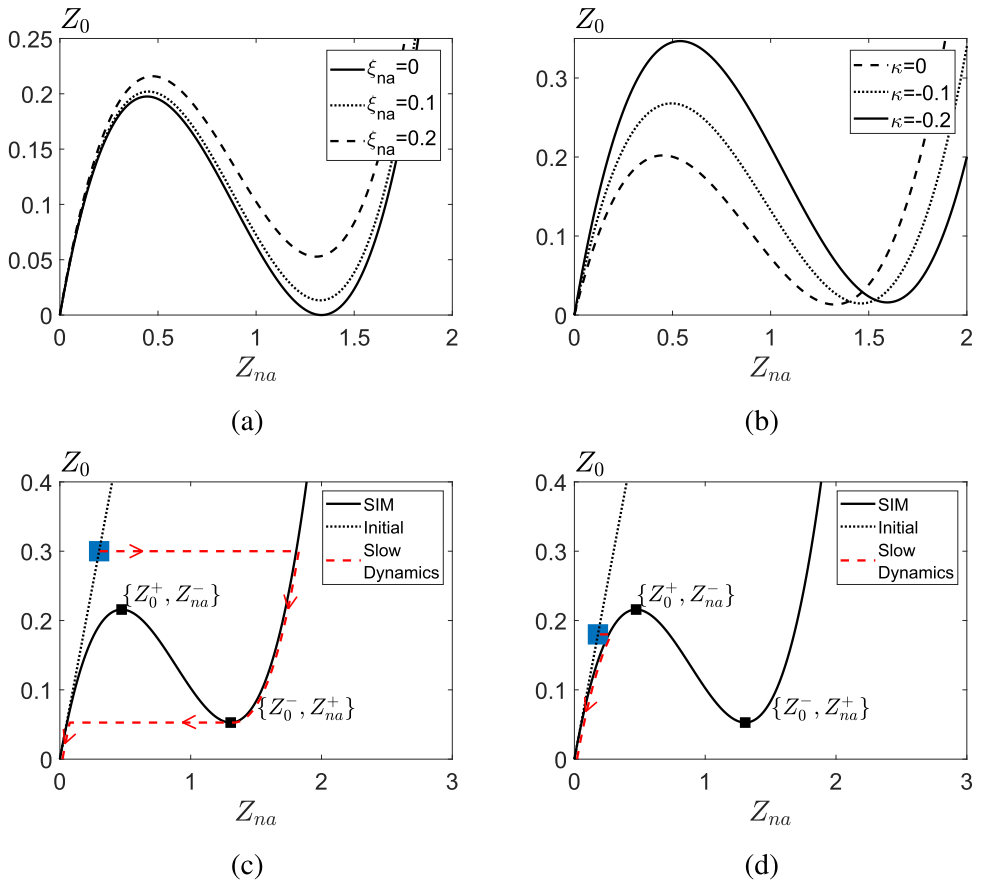

Fig. 4. The SIM for $\kappa = 0$ and several ξ_{na} (a) and for $\xi_{na} = 0.1$ and several κ. Attraction to the right (c) and left branch (d).

To initiate on the right branch and thus ensure TET, it needs to be understood how the initial conditions of x_ℓ and x_{na} initiate on the $Z_{na}Z_0$-plane. As the initial conditions can be chosen arbitrarily, and so are not related by the SIM, the dynamics can initiate anywhere on the $Z_{na}Z_0$-plane. Because the SIM describes the dynamics on the slow time scale, the actual dynamics still need to be attracted to the SIM.

By only considering shock loads, the initial conditions are modeled as an impulsive excitation, where only the main system has an initial speed, $u(0) = v(0) = 0, \dot{x}_\ell(0) \neq 0, x_\ell(0) = \dot{x}_{na}(0) = 0$ then $\dot{u} = \dot{v} = \dot{x}_\ell(0)$.

With $Z_0(0) = \Omega_3(\dot{u}_0^2(0) + \omega_i^2 u_0(0))$ and $Z_{na}(0) = \Omega_3(\dot{v}_0^2(0) + \omega_i^2 v_0(0))$, an impulsive excitation will initiate on the line $Z_0 = Z_{na}$ through the origin in the $Z_{na}Z_0$ plane. This line is plotted together with a SIM in Fig. 4c and d. When $Z_0(0) > Z_0^+$ in Fig. 4c, the dynamics will be attracted to the right branch. This condition for TET for a NES was found in previous works as well, and is confirmed by numerical simulations of (6) [2,3,22]. When $Z_0^- < Z_0(0) < Z_0^+$ the dynamics can either be attracted to the slow left branch or the optimal right branch. In Fig. 4d, the line of initial conditions is very close to the left branch. Therefore, the dynamics will be attracted to this slow, suboptimal branch. This was also confirmed by simulations in Refs. [2,22]. It can be concluded that $Z_0(0) > Z_0^+$ is the condition to trigger TET under impulsive excitation. To meet this condition, NES coefficient should be tuned as follows:

$$Z_0(0) > Z_0^+ \rightarrow k_{na} \geq \frac{m_{na}\omega_i^4(Z_0^+)}{\dot{u}^2(0) + \omega_i^2 u^2(0)} \tag{10}$$

3.4. Performance

The performance measures here are based on slow flow dynamics (8). These are simulated for $\xi_{na} = 0.1$ and $\kappa = \xi = 0$, once for $Z_0(0) = 0.22 > Z_0^+$ on the right branch, and once for $Z_0(0) = 0.2 < Z_0^+$ on the left branch.

The slow time evolution of Z_0 and Z_{na} are shown in Fig. 5. When $Z_0(0) = 0.22$, Z_0 drops rapidly until there is a sudden change of the slope. The corresponding Z_{na} on the other hand drops slowly until there is a sudden drop in value. This happens at the same time of the slope change of Z_0. This duration of efficient energy transfer, where Z_0 drops rapidly, is what will be called

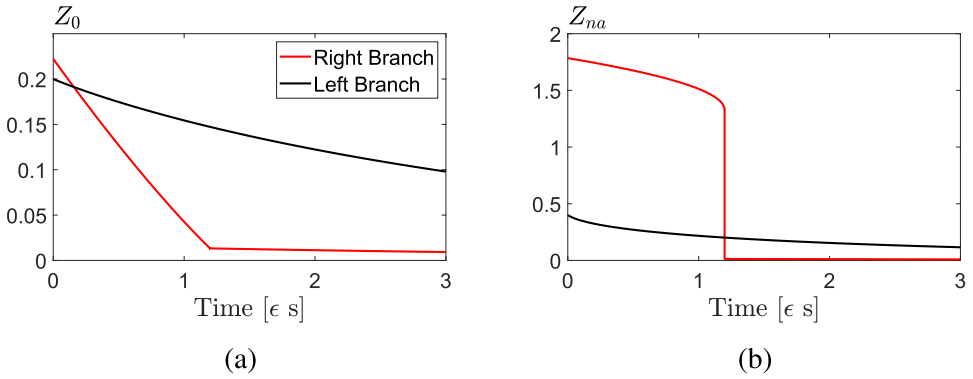

Fig. 5. Slow flow dynamics time evolution for $\kappa = 0$ and $\xi_{na} = 0.1$ with $Z_0(0) = 0.22$ (red) and $Z_0(0) = 0.2$ (black). (For interpretation of the references to colour in this figure legend, the reader is referred to the Web version of this article.)

pumping time. After the change of slope, there is residual energy left (Z_0^-). For $Z(0) = 0.20$, Z_0 initiates on the left branch and both Z_0 and Z_{na} decay rather slowly.

Next, the pumping time and residual energy will be expressed in static formulas, instead of determined by numerical simulations of (8). These are the algebraic performance measures, to stress no simulation is required to obtain the pumping time and residual energy, only knowledge of the system's parameters.

3.4.1. Energy dissipation

When initiated, TET persists until the slow dynamics reach the local minimum of the SIM. At this point, not all of the vibration energy has been dissipated. The fractional residual energy is

$$E_{res} = \frac{Z_0^-}{Z_0(0)} = \frac{E_0^-}{E_0(0)} \tag{11}$$

with its complement the fraction of the initial energy dissipated by the NES during TET:

$$E_{TET} = 1 - \frac{Z_0^-}{Z_0(0)} = 1 - \frac{E_0^-}{E_0(0)} \tag{12}$$

Both $Z_0(0) = \Omega_3(\dot{u}(0)^2 + \omega_i^2 u^2(0))$ and Z_0^-, (9), depend only on the mechanical system's and NES's parameters, there is no need to simulate (8) to determine the residual or dissipated energy.

The amount of energy dissipated by the NES is often the only performance measure that is considered in literature. Unlike here, it is typically calculated numerically from simulations or experiments.

For the amplitude, analogous performance measures can be defined:

$$A_{res} = \frac{\sqrt{Z_0^-}}{\sqrt{Z_0(0)}} = \frac{\sqrt{E_0^-}}{\sqrt{E_0(0)}} \tag{13}$$

with its complement:

$$A_{TET} = 1 - \frac{\sqrt{Z_0^-}}{\sqrt{Z_0(0)}} = 1 - \frac{\sqrt{E_0^-}}{\sqrt{E_0(0)}} \tag{14}$$

3.4.2. Pumping time

The SIM and slow flow dynamics (8) can be combined to yield an expression for $\frac{\partial Z_{na}}{\partial T_1}$. By assuming a lightly damped main system, $\xi \approx 0$, separation of variables allows for integration. This results in:

$$\overbrace{\frac{27}{32}Z_{na}^2 - 3(1-\kappa)Z_{na} + \left((1-\kappa)^2 + \xi_{na}^2\right)\ln(Z_{na})}^{I(Z_{na})} = C - \omega_i \xi_{na} T_1 \tag{15}$$

From (15), the duration (in slow time) between two states of Z_{na} on the SIM can be calculated. If TET is initiated, the SIM will be descended from $Z_{na}(0)$ to Z_{na}^+, as depicted in Fig. 4c. The duration of TET, called pumping time, is thus:

$$\varepsilon T_{pump} = \frac{1}{2\pi\xi_{na}}\left(I(Z_{na}(0)) - I(Z_{na}^+)\right) \tag{16}$$

with T_{pump} relative to the period of the modal frequency and $T_{pump}\frac{\omega_i}{2\pi}$ the time in seconds. A more elaborate derivation is found in Ref. [3]. As with the previous performance measures, the novelty is that the pumping time here only depends on the system's parameters.

Caution needs to be taken to determine $Z_{na}(0)$. As (15) assumed dynamics are on the SIM, $Z_{na}(0)$ has to be on the SIM. For this, $Z_{na}(0)$ is chosen as the Z_{na} on the SIM corresponding with $Z_0(0)$.

In Refs. [3,23] it was shown that T_{pump} is a valid estimation for the duration of efficient energy transfer to the NES, when compared to actual numerical simulations of (6).

3.4.3. Cascading time

When the mechanical system vibrates with its modal frequencies, a NES can engage in RCC. The duration of RCC can be estimated by the sum of the individual modes' pumping time. To extend the pumping time to multi-modal vibrating systems, the initial modal conditions are considered. The initial condition on $\mathbf{x}$ can be decomposed in the initial conditions of each mode:

$$\dot{\mathbf{x}}(0) = \sum_{k=1}^{n} \dot{\mathbf{x}}^{[k]}(0) = \sum_{k=1}^{n} \mathbf{e_k}\dot{q}_k(0), \tag{17}$$

with $\dot{\mathbf{x}}^{[k]}(0) = \mathbf{e}_k\dot{q}_k(0) \in \mathbb{R}^n$ the hypothetical initial speed as if only mode k is present. The initial displacements can similarly be expressed as $x^{[k]}(0) = e_k q_k(0) \in \mathbb{R}^n$. By considering each mode separately, $\dot{x}_{\ell}^{[k]}(0)$ can be used to calculate a $Z_0(0)$ allowing to tune the NES, (10), and calculate the performance (12, 16) for each mode.

During resonance capture cascade (RCC), only a single mode is interacting with the NES at a given time. Therefore, in Ref. [3] it was hypothesized that the total duration of the cascade is the sum of the pumping times of each contributing mode. Further numerical simulations validated this hypothesis [3,23].

The cascading time is then:

$$T_{cascade} = \sum_{i=1}^{k} T_{pump}^{[i]} \cdot \frac{\omega_i}{2\pi} \tag{18}$$

As each individual pumping time is calculated without simulation, so is the cascading time.

4. Experimental setup and identification

4.1. Restoring force surface method

The restoring force surface (RFS) method was introduced in Ref. [24] as a graphical tool to detect nonlinear restoring forces in dynamical systems. Recently, it was adopted in experimental structural dynamics [20,21] to detect and visualize mechanical nonlinearities. A discrete nonlinear mechanical system is subjected to Newton's second law and has the following structure:

$$m\ddot{q} = p + f(q, \dot{q}) \tag{19}$$

with q its degree of freedom, $m\ddot{q}$ the inertial term, p an external force and $f(q, \dot{q})$ the restoring forces, consisting of stiffness and dissipative forces. If p, q, $\dot{q}$ and $\ddot{q}$ are available through measurement, the restoring force is given by a surface in $(q, \dot{q})$:

$$f(q, \dot{q}) = m\ddot{q} - p \tag{20}$$

For each instant, there is a triplet $q(t), \dot{q}(t), m\ddot{q}(t) - p(t)$. If enough data is captured, an experimental surface can be constructed with these triplets. Cross sections of this surface, where either $\dot{q} \approx 0$ or $q \approx 0$, will then graphically display the stiffness forces and the damping forces respectively.

4.2. Identification of NES

The realized NES is fixed to a shaking table, Fig. 2b, being a linear motor (Beckhoff AL2012) controlled by a PLC (Beckhoff CX5210). The imposed motion of the shaking table is a sine sweep. This motion is a ground displacement z to the NES. We express (3) in the relative ground coordinate $q \triangleq x - z$:

$$m\ddot{q} + m\ddot{z} = -c\dot{q} - kq - k_3q^3 \tag{21}$$

Relating (20) to (21), the external excitation is $p = -m\ddot{z}$ and the restoring force surface is $f(q, \dot{q}) = -c\dot{q} - kq - k_3q^3$. To experimentally construct the surface, the NES and shaking table are fitted with accelerometers, measuring $\ddot{z}$ and $\ddot{q}$. The other variables q and $\dot{q}$ are obtained by integrating the $\ddot{q}$ once and twice respectively. The measured $\ddot{q}$ and $\ddot{z}$ are shown for a selected range in Fig. 6b and a. This range is used for the RFS-method and selected because of the high amplitude of both $\ddot{q}$ and $\ddot{z}$, to avoid noise and static friction effects of the mechanism introduced by the surface contact between follower and force profile. The integrated signals $\dot{q}$ and q are shown in Fig. 6c and d.

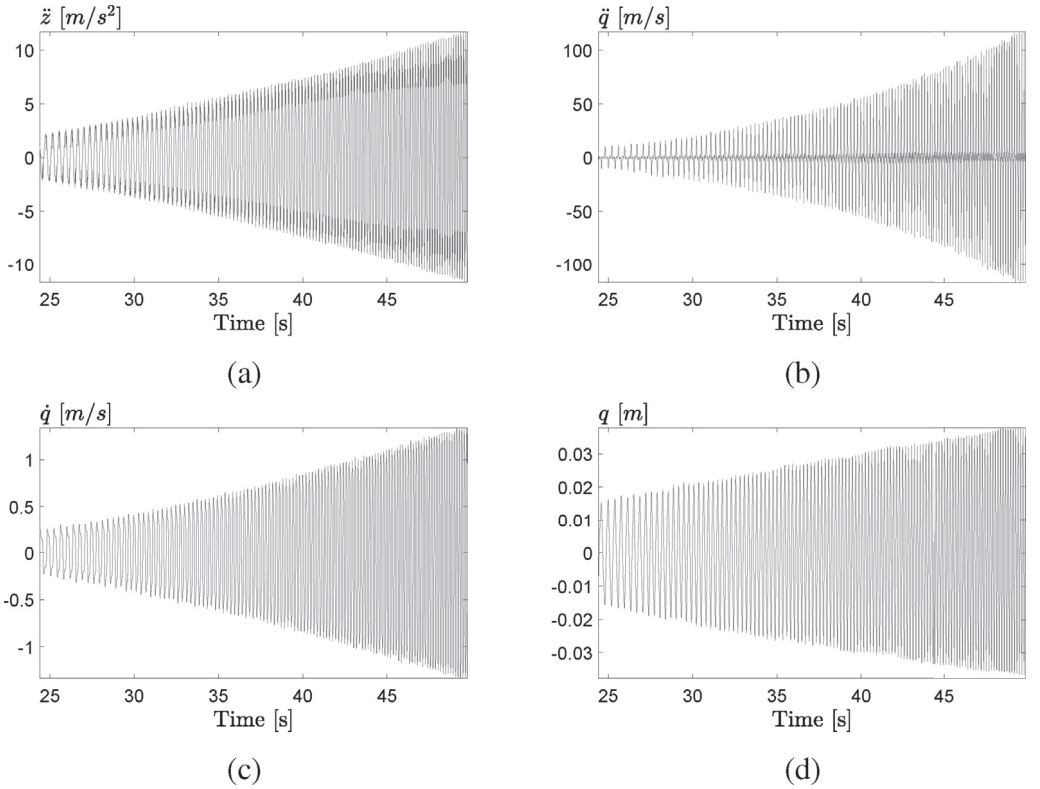

Fig. 6. Measured acceleration with (a) the ground acceleration and (b) the relative absorber acceleration, (c) and (d) are the numerical integration and twice integration of the relative absorber acceleration.

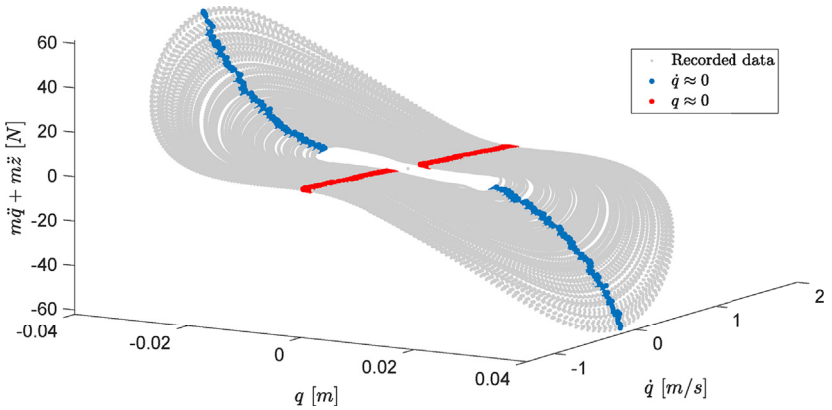

Fig. 7. Experimental restoring force surface with highlighted ranges of $q \approx 0$ and $\dot{q} \approx 0$.

Shown in Fig. 7 are the available triplets $q(t), \dot{q}(t), p(t) - m\ddot{q}(t)$ in the selected range. Cross sections are highlighted where $\dot{q} = [-0.03, 0.03] \approx 0$, and $q = [-0.0012, 0.0012] \approx 0$. The collection of points in these cross sections are plotted in Fig. 8a for stiffness and Fig. 8b for damping. On these points, $-k_3 q^3$ is fitted for the stiffness and $-c\dot{q}$ for the damping by minimizing the least-squared-error. The obtained results are $k_3 = 1.1504 \cdot 10^6$ N m^{-3} and $c = 2.1714$ N m^{-1}. The NES mechanism was designed to have a $k_3 = 1.07 \cdot 10^6$ N m^{-3}. This slight deviation is attributed to manufacturer tolerances on the linear spring and on the machined force profile.

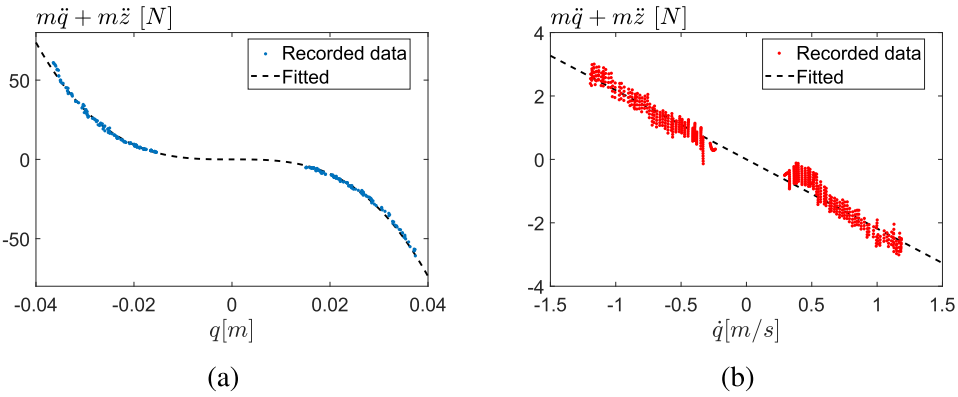

Fig. 8. The cross sections highlighted on the experimental RFS Fig. 7, with (a) the stiffness force and (b) the damping force.

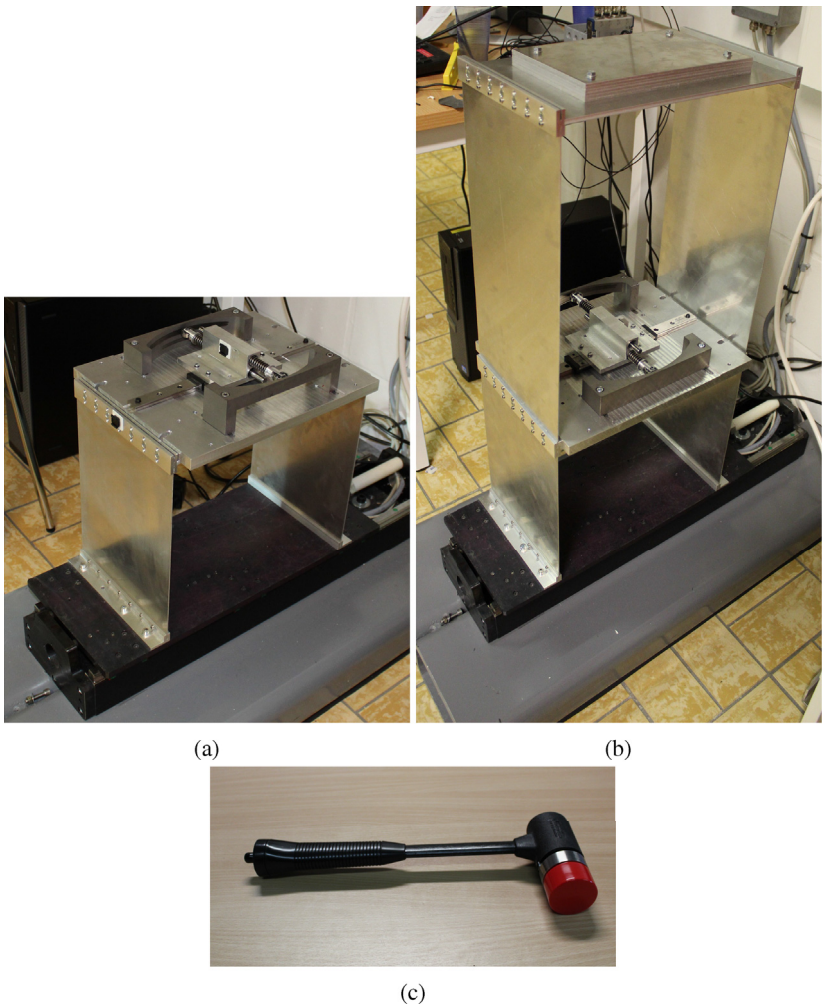

Fig. 9. Picture of the frame (main system) with NES mechanism on top (a) and impact hammer used to measure impact force (c).

4.3. Identification of the mechanical system

The mechanical systems used in the experiments are depicted in Fig. 9a and b with the NES already attached. The first is a single aluminum frame, representing an SDOF system. In the second setup, a second frame is put on the first to create a 2DOF

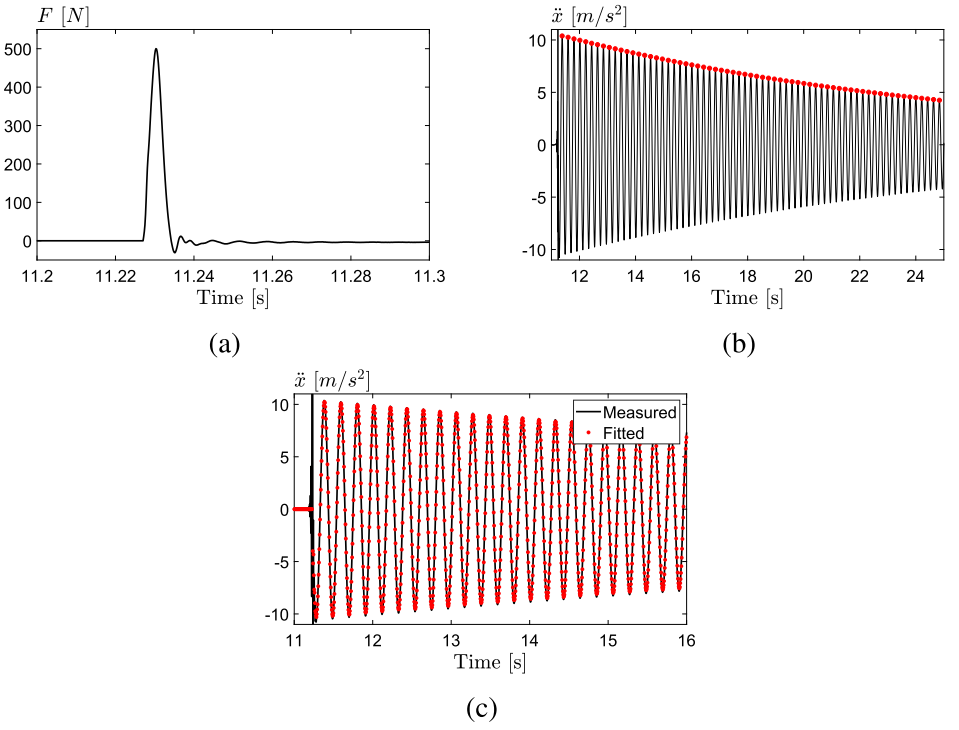

Fig. 10. The experimental free response with the local extrema marked (b) and (c) the fitted SDOF response.

system having two dominant vibration modes. A single shear frame can be modeled as a single mass-spring-damper system with the top mass displacement as the coordinate. The two frames will now be identified separately with the NES detached.

4.3.1. Shear frame model

A shear frame can be modeled as a mass-spring-damper system, provided it has a large top mass relative to the wall mass and if the walls are ideally clamped at both the bottom and the top. The top mass of the first frame weighs 5.11 kg, significantly heavier than the wall mass that weighs 0.21 kg.

The stiff walls deflect if a force is acting upon the top mass. The equivalent stiffness of a single wall under shear based idealization is:

$$k_{eq} = \frac{Et^3 w}{L^3} \tag{22}$$

with E Young's modulus (69 G pa), t the thickness of the wall (1.5 mm), w the width (200 mm) and L its length (250 mm for the first frame). The total stiffness for both walls of the first frame is 5.69 k N m^{-1}.

The equivalent mass m_{eq} of a shear frame has a contribution of the top mass and part of the wall's mass:

$$m_{eq} = m_{floor} + \frac{1}{3} m_{walls} \tag{23}$$

or $m_{eq} = 5.25$ kg for the first frame. With an equivalent mass and stiffness, this frame has an expected natural frequency of $\omega_n = 33.7$ rad s^{-1}. The natural frequency, equivalent mass and damping are now experimentally determined.

4.3.2. Experimental parameters frame 1

To experimentally identify the parameters, the frame was subjected to an impact on the top mass. This was applied by an impact hammer, see Fig. 9c, which records the applied impact force. See Fig. 10a for such a recording. The resulting free vibration of the frame was captured by an accelerometer on the top mass, see Fig. 10b for a filtered version of this recording. The local extrema T_i are used to calculate the period T_n and the logarithmic decrement Λ:

$$T_{n,i} = T_{i+1} - T_i \qquad \Lambda_i = \ln \frac{T_i}{T_{i+1}} \tag{24}$$

with $\Lambda \approx 2\pi\zeta$, ζ the damping ratio. The period and logarithmic decrement were averaged, with the resulting natural frequency and damping ratio of the experiment reported in Table 1. The deviation between theoretical and experimental natural frequency is attributed to the non-ideal clamping condition.

Table 1
The equivalent parameters of the first frame, both theoretical and experimental.

Parameter	Theoretical frame 1	Experimental frame 1
ω_n [rad s^{-1}]	33.7	29.2
ζ [–]	–	0.0022
m_{eq} [kg]	5.25	5.29

Table 2
The identified parameters of the NES and the two shear frames.

Parameter	Value
m_1 [kg]	5.29
k_1 [N m^{-1}]	4738
c_1 [N s m^{-1}]	0.66
m_2 [kg]	2.75
k_2 [N m^{-1}]	1432
c_2 [N s m^{-1}]	0.22
m_{na} [kg]	0.49
k_3 [N m^{-3}]	$1.1504 \cdot 10^6$
c_{na} [N s m^{-1}]	2.17

To obtain the equivalent mass, the differential equation of the equivalent SDOF frame model with experimental parameters was simulated, with the recorded impact (Fig. 10a) as input $F(t)$:

$$\ddot{x} + 2\zeta\omega_n\dot{x} + \omega_n^2 x = \frac{F(t)}{m_{eq}} \tag{25}$$

with the m_{eq} adjusted so that the root mean squared error between the recorded and simulated response is minimized. The result for $m_{eq} = 5.29$ is plotted in Fig. 10c.

4.3.3. Experimental parameters frame 2

A second shear frame was used to create an experimental 2DOF system by stacking it on the 1st frame. Only its experimental parameters are determined here. This frame has a height of 380 mm and same width and thickness as the first frame. To identify the equivalent parameters of frame 2, this frame itself was fixed to the ground and the same procedure as for frame 1 was applied to obtain the SDOF parameters of frame 2. The experimental parameters of both frames are given in Table 2 with m_1, k_1 and c_1 obtained from the first frame and m_2, k_2 and c_2 from the second. The second frame is stacked on the first frame in the next section. The 2DOF main system is assumed to have the following structure:

$$\mathbf{M} = \begin{bmatrix} m_1 & 0 \\ 0 & m_2 \end{bmatrix} \mathbf{K} = \begin{bmatrix} k_1 + k_2 & -k_2 \\ -k_2 & k_2 \end{bmatrix} \mathbf{C} = \begin{bmatrix} c_1 + c_2 & -c_2 \\ -c_2 & c_2 \end{bmatrix} \tag{26}$$

From the above matrices and the parameters in Table 2, the eigenfrequencies and -vectors are:

$$\mathbf{E} = \begin{bmatrix} \mathbf{e}_1 & \mathbf{e}_2 \end{bmatrix} = \begin{bmatrix} 0.184 & 0.38 \\ 0.542 & -0.264 \end{bmatrix} \quad \begin{bmatrix} \omega_1 \\ \omega_2 \end{bmatrix} = \begin{bmatrix} 18.54 \\ 35.54 \end{bmatrix} \text{ rad s}^{-1} \tag{27}$$

The two frames were constructed so that the eigenfrequencies of the two-frame structure are not too far apart. For closer eigenfrequencies, the cascading of all modes is shorter than if they are further apart [3].

5. Experimental performance

5.1. Expected performance

Before carrying out any experiments or simulations, the NES performance is estimated with (12), (16) and (18) using the identified parameters in Table 2 and proposing the initial energy. From the identified parameters, ϵ, ξ_{na}, ω_i, Ω_3 and Z_0^+ are given in Table 3 for both the single and double frame structure. These allow for a more direct calculation of the performance by the reader.

For the single frame, the minimal initial speed to trigger TET is $\dot{x}(0) = 0.25$ m s^{-1}, computed from the condition $Z_0(0) > Z_0^+$, with $Z_0(0) = \Omega_3\dot{x}(0)^2$. TET is fastest near $Z_0(0) = Z_0^+$, with a pumping time of 0.3 s, yet only a dissipation energy of 0.85. This corresponds to a significant residual amplitude A_{res} of 0.39. The NES performance for $\dot{x}(0) = [0.25, 1]$ m s^{-1} is shown in Fig. 11a. As $\dot{x}(0)$ increases, so does the pumping time, while more energy is dissipated. The NES performance thus is a choice between

Table 3
Parameters used to calculate performance.

Frame 1	ε	ξ_{na}	ω_n	Ω_3	Z_0^+
	0.088	0.152	29.2	3.24	0.208
Frame 1 & 2	ε_i	$\xi_{na,i}$	ω_i	$\Omega_{3,i}$	$Z_{0,i}^+$
mode 1	0.017	0.238	18.6	20.72	0.224
mode 2	0.070	0.125	35.5	1.53	0.205

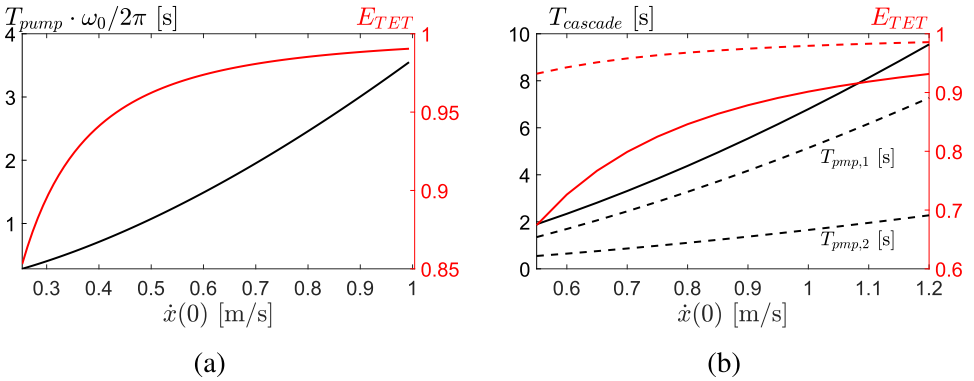

Fig. 11. The predicted performance of the NES for single frame (a) and two frame (b) mechanical system, with red dash E_{TET} for mode 2 and red solid E_{TET} for mode 1. (For interpretation of the references to colour in this figure legend, the reader is referred to the Web version of this article.)

either faster TET or less residual energy. The reason for this is that, as $Z_0(0)$ is more and more above the threshold Z_0^+, a larger part of the SIM is descended, as seen in Fig. 4c. This will cause the pumping time to increase while, also increasing the dissipated energy as the fraction $\frac{Z_0(0)}{Z_0^-}$ decreases.

For the double frame structure, the shock will be applied to the bottom frame. The condition $Z_0(0) > Z_0^+$ is met for both modes for an initial speed $x_1(0)$ of 0.53 m s^{-1}. The NES performance for the range $\dot{x}_1(0) = [0.53, 1.2]$ m s^{-1} is given in Fig. 11b, with the cascading time being the sum of the pumping times of the two individual modes. The energy dissipation per mode is also given. The cascading time is shortest on the threshold (about 2 s), yet the NES energy dissipation is low, especially for the 1st mode with 0.67 or a residual amplitude of 0.57. Analogous to the single frame case, increasing the initial speed increases the cascading time, but a greater amount of energy will be dissipated. Later, experiments will verify the performance predicted here.

5.2. Design of experiment

The performance measures were derived under the assumption of an unforced mechanical system under initial conditions. In the experiments, the impact hammer in Fig. 9c is used to apply a shock load to the frame. This impact expressed in an equivalent initial speed, provided the duration of the impact is significantly shorter than the natural period of the structure. As seen in Fig. 10a, the force duration is indeed magnitudes shorter (less than 0.01 s) than the natural period of $T_n = 0.21$ s. The equivalent initial speed from a short force recording $F(t)$:

$$\dot{x}(0)_{eq} = \frac{I}{m} = \frac{\int_0^{t_d} F(t)dt}{m_{eq}} \tag{28}$$

Table 4
The performance of the NES for the single frame expressed in pumping time and energy dissipation.

$\dot{x}(0)$ [m s^{-1}]	$Z_0(0)$	E_{TET}	T_{pump} [s]	$T_{pmp,exp}$ [s]	%
0.39	0.5027	0.940	0.69	0.86	20%
0.60	1.163	0.974	1.48	1.64	9%
0.80	2.10	0.985	2.48	2.62	5%
0.13	0.0562	–	–	–	

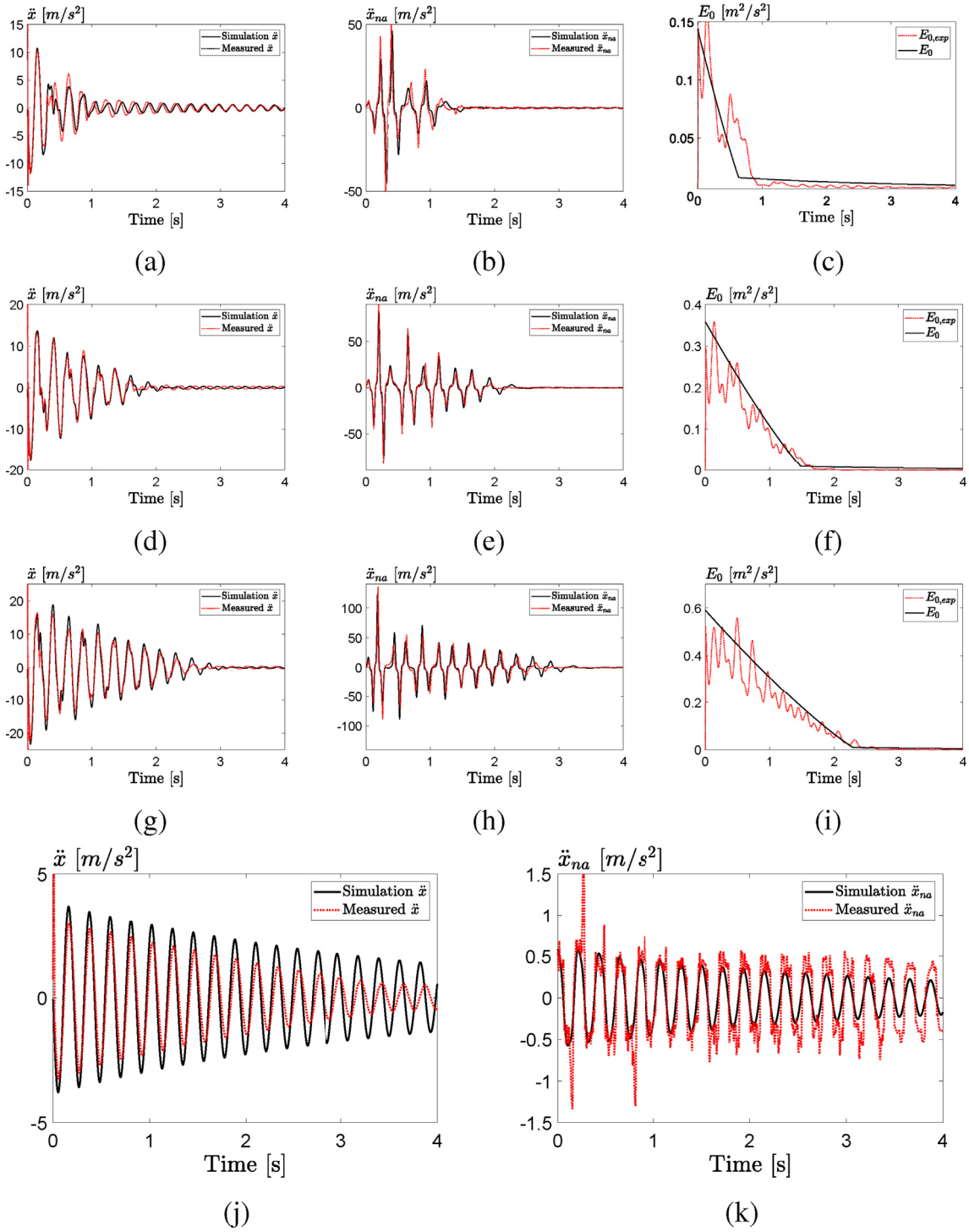

Fig. 12. Experimental results of NES on the single frame. With (a),(d) and (g) frame acceleration, (b),(e) and (h) NES acceleration and (c),(f) and (i) the energies for increasing impact. Frame impacted below the threshold (j) and (k).

with I the intensity of the force, t_d the duration of the pulse and m_{eq} the equivalent impacted mass.

During the experiment the main system is impacted on the first frame with varying intensities and the acceleration of both the NES and the main system is measured. The measured acceleration will be compared with the simulated acceleration, obtained by simulating (6) with the equivalent initial speed.

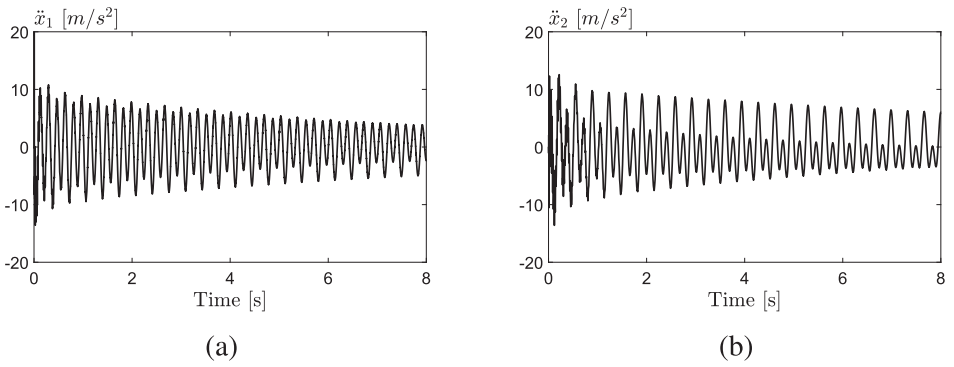

Fig. 13. Measured accelerations of first (a) and second floor (b) of the building frame without NES subjected to an impact.

5.3. Experiments single mode

The acceleration of the single frame without the NES has been plotted before in Fig. 10b. These vibrations will now be mitigated by fitting the SDOF frame with the NES, Fig. 9a. The frame is subjected to impact of increasing magnitudes. The equivalent speed of the impacts along with the estimated performance are given in Table 4. Fig. 12a, d, g and j show the acceleration on the frame and Fig. 12b, e, h, k show the NES acceleration. As Fig. 11a predicted, the harder the frame is impacted, the longer the duration of targeted energy transfer, but the less residual energy. For the weakest impact, Fig. 12j and k, the initial energy is below the energy threshold Z_0^+. As a consequence, there is no TET. Even though the NES mitigates the vibrations suboptimally, the dissipation is still a lot faster than the frame without the NES, Fig. 10b. The simulations overlayed on the measurement show good accordance with the experiments.

The estimated performance is now compared to the experimental performance by comparing $E_{0,exp}$, the vibration energy from the experiment, with the slow flow E_0, simulated from (8). $E_{0,exp}$ is calculated from the experimental vibrations:

$$E_{0,exp} = \dot{x} - \dot{x}_{na} + \omega_n(x - x_{na}) \tag{29}$$

with the displacement and speed integrated from the acceleration. The comparison of E_0 and $E_{0,exp}$ is made in Fig. c, f and i. The experimental pumping time $T_{pump,exp}$ is the time at which $E_{0,exp}$ is decayed to the level of the dissipated energy E_{TET}, and is given in Table 4. The $T_{pump,exp}$ is consistently higher than the expected T_{pump}. Although the % difference decreases for increasing strength of impact, the absolute difference is more or less constant. The same observation was made in Ref. [23], where the pumping time of numerical simulations of (6) was compared to the pumping time of (16). The longer experimental and numerical pumping time is attributed to the attraction phase of the fast dynamics to the SIM, as discussed in Section 3.3, while calculating the pumping time with (16) assumes the dynamics are already on the SIM.

5.4. Experiments two modes

The second frame is attached to the first frame and the experiment is repeated. The impact force is applied to the first frame mass to obtain vibrations in both modes. First, the two-frame building is impacted without the NES. The vibrations of the first and second frame, Fig. 13a and b decay very slowly.

With the NES attached, impacts with increasing higher intensity are applied, with Figs. 14a, 15a and 16a the NES acceleration, Figs. 14c, 15c and 16c the acceleration of the first frame and Figs. 14c, 15d and 16d the acceleration of the second frame. Simulations of the 2DOF + NES system are also plotted in the figures and show a good accordance. For the applied impacts, the performance calculated from (12) and (18) is found in Table 5. The resonance cascade is observed, as the NES first vibrates with the frequency of the 2nd mode and then cascades to the first mode. To further highlight the sequential mitigation of the vibration modes during the resonance cascade, the wavelet transform of the experimental NES acceleration is shown on Figs. 14b, 15b and 16b. The wavelet transform is able to track the frequency over time. Each mode engages in TET for about its estimated pumping time, confirming that the cascading time is estimated by summing the individual pumping times. The frames first vibrate in both modes. During the pumping of the second mode, this mode is mitigated. The first mode remains and decays until some residual energy is left.

A quantitative comparison of experimental and predicted cascading time is not possible, as $E_{0,exp}$ of modes 1 and 2 cannot be separated. However, the wavelet transform qualitatively confirms the validity of the cascading time as a performance measure.

6. Conclusion

The practical use of a nonlinear energy sink (NES) in mitigating transient vibration energy in a mechanical system has been given a comprehensive engineering treatment, from proposed design to actual implementation and placement on a physical

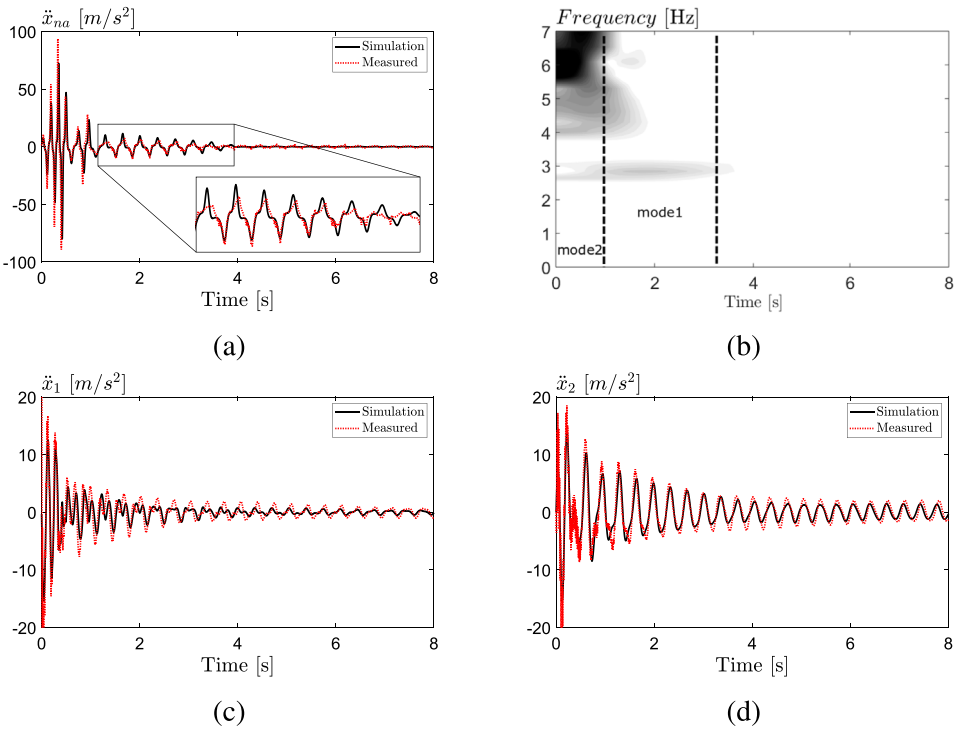

Fig. 14. For $\dot{x}_1(0) = 0.60$ m s^{-1}, the measured and simulated acceleration of NES (a), its Wavelet transform (b), first (c) and second floor (d).

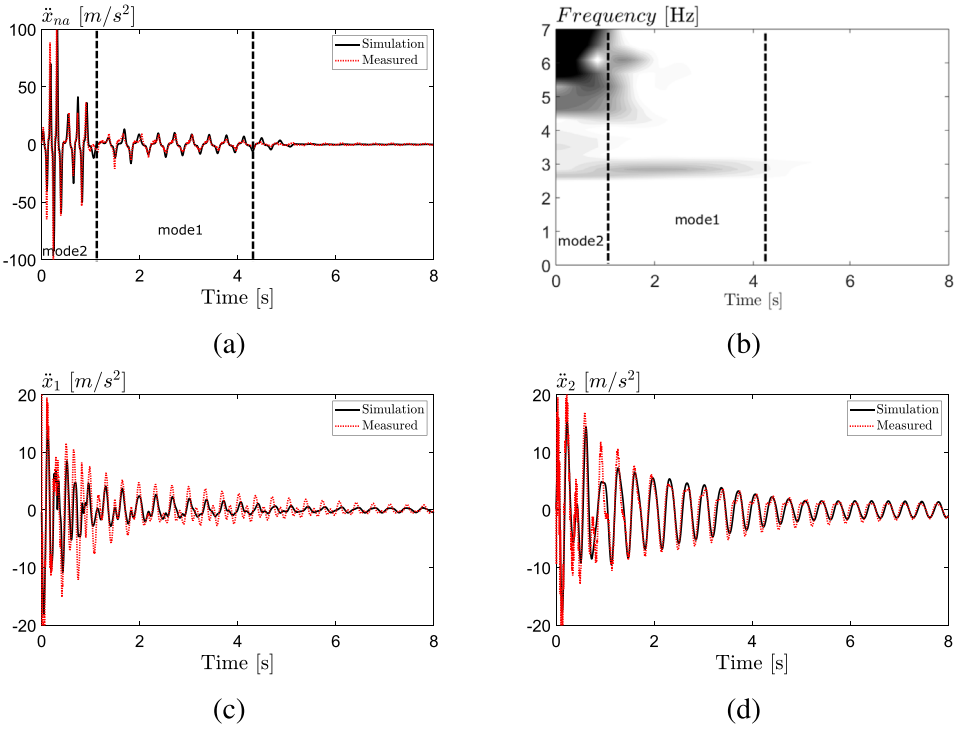

Fig. 15. For $\dot{x}_1(0) = 0.71$ m s^{-1}, the measured and simulated acceleration of NES (a), its Wavelet transform (b), first (c) and second floor (d).

setup. The NES has been realized with an axial spring that follows a machined nonlinear track. This track ensured a purely cubic stiffness characteristic, which was verified by identification of the NES, using the restoring force surface method. The NES was

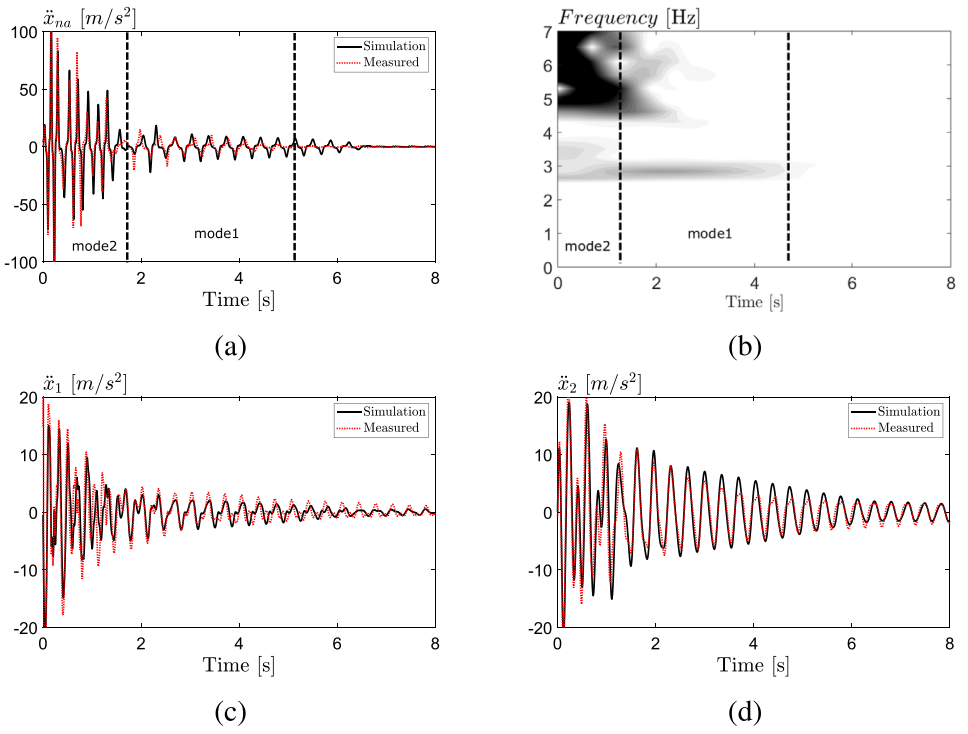

Fig. 16. For $\dot{x}_1(0) = 0.88$ m s^{-1}, the measured and simulated acceleration of NES (a), its Wavelet transform (b), first (c) and second floor (d).

Table 5
Performance of the NES tuned for the 2DOF system.

$\dot{x}_1(0)$	$\dot{q}_2(0)$	$\dot{q}_1(0)$	$T^{[2]}_{pmp}\frac{\omega_2}{2\pi}$ [s]	$T^{[1]}_{pmp}\frac{\omega_1}{2\pi}$	T_{csc}	$E^{[2]}_{TET}$	$E^{[1]}_{TET}$
0.60	1.29	0.63	0.65	1.72	2.37	0.94	0.78
0.71	1.52	0.74	0.89	2.5	3.40	0.96	0.8
0.88	1.90	0.93	1.31	3.98	5.29	0.97	0.87

then fitted to a frame, which represented a single-mode vibrating system. By impulsively loading the frame with an impact hammer, the NES engaged in targeted energy transfer. The frame-NES system behaved in accordance with simulations of the identified model. Both the duration of TET and the residual energy were predicted well by the performance measures. A second frame was attached, creating a two-mode mechanical system. When the two-frame system was impacted, the NES engaged in resonance capture cascade, where both modes of the two-frame system were sequentially mitigated. The prediction of the NES performance with cascading time was also experimentally verified. This work has solidified the feasibility of the NES in mitigating single and multi-modal vibrations in real life structures, and the ability of the performance measures (pumping time, residual energy and cascading time) in predicting the performance of the NES without the need of time consuming simulation or experimental campaigns.

Author contribution

Kevin Dekemele: Conceptualization, Methodology, Software, Writing - Original Draft, Visualization, Investigation, Formal analysis. **Patrick Van Torre:** Supervision, Project administration, Resources. **Mia Loccufier:** Supervision, Project administration, Resources, Formal analysis, Writing - Review & Editing

Declaration of competing interest

None.

Acknowledgement

The authors would like to express our great appreciation to Michiel Dhont who assisted in the realization of the NES and development of the identification software.

References

[1] A.F. Vakakis, O.V. Gendelman, L.A. Bergman, M.D. McFarland, G. Kerschen, Y.S. Lee, Nonlinear Targeted Energy Transfer in Mechanical and Structural Systems, Springer Netherlands, 2009.
[2] T.A. Nguyen, S. Pernot, Design criteria for optimally tuned nonlinear energy sinkspart 1: transient regime, Nonlinear Dynam. 69 (12) (2012) 1–19.
[3] K. Dekemele, R. De Keyser, M. Loccufier, Performance measures for targeted energy transfer and resonance capture cascading in nonlinear energy sinks, Nonlinear Dynam. 93 (2) (2018) 259–284, https://doi.org/10.1007/s11071-018-4190-5.
[4] G. Kerschen, Y.S. Lee, A.F. Vakakis, M.D. McFarland, L.A. Bergman, Irreversible passive energy transfer in coupled oscillators with essential nonlinearity, SIAM J. Appl. Math. 66 (2006) 648–679.
[5] A. Tripathi, P. Grover, T. Kalmr-Nagy, On optimal performance of nonlinear energy sinks in multiple-degree-of-freedom systems, J. Sound Vib. 388 (2017) 272–297.
[6] A.F. Vakakis, L. Manevitch, O. Gendelman, L. Bergman, Dynamics of linear discrete systems connected to local, essentially non-linear attachments, J. Sound Vib. 264 (3) (2003) 559–577.
[7] G. Kerschen, J.J. Kowtko, D.M. McFarland, L.A. Bergman, A.F. Vakakis, Theoretical and experimental study of multimodal targeted energy transfer in a system of coupled oscillators, Nonlinear Dynam. 47 (1) (2007) 285–309.
[8] G. Kerschen, A.F. Vakakis, Y.S. Lee, D.M. Mcfarland, J.J. Kowtko, L.A. Bergman, Energy transfers in a system of two coupled oscillators with essential nonlinearity: 1: 1 resonance manifold and transient bridging orbits, Nonlinear Dynam. 42 (3) (2005) 283–303.
[9] D.M. McFarland, G. Kerschen, J.J. Kowtko, Y.S. Lee, L.A. Bergman, A.F. Vakakis, Experimental investigation of targeted energy transfers in strongly and nonlinearly coupled oscillators, J. Acoust. Soc. Am. 118 (2) (2005) 791–799.
[10] D.M. McFarland, L.A. Bergman, A.F. Vakakis, Experimental study of non-linear energy pumping occurring at a single fast frequency, Int. J. Non Lin. Mech. 40 (6) (2005) 891–899.
[11] G. Kerschen, D.M. McFarland, J.J. Kowtko, Y.S. Lee, L.A. Bergman, A.F. Vakakis, Experimental demonstration of transient resonance capture in a system of two coupled oscillators with essential stiffness nonlinearity, J. Sound Vib. 299 (45) (2007) 822–838.
[12] A.T. Savadkoohi, B. Vaurigaud, C.-H. Lamarque, S. Pernot, Targeted energy transfer with parallel nonlinear energy sinks, part ii: theory and experiments, Nonlinear Dynam. 67 (1) (2012) 37–46.
[13] C.-H. Lamarque, A.T. Savadkoohi, S. Charlemagne, Experimental results on the vibratory energy exchanges between a linear system and a chain of nonlinear oscillators, J. Sound Vib. 437 (2018) 97–109.
[14] L.I. Manevitch, E. Gourdon, C.-H. Lamarque, Towards the design of an optimal energetic sink in a strongly inhomogeneous two-degree-of-freedom system, J. Appl. Mech. 74 (6) (2007) 1078–1086.
[15] J. Luo, N.E. Wierschem, L.A. Fahnestock, L.A. Bergman, B.F. Spencer Jr., M. Al-Shudeifat, D.M. McFarland, D.D. Quinn, A.F. Vakakis, Realization of a strongly nonlinear vibration-mitigation device using elastomeric bumpers, J. Eng. Mech. 140 (5) (2013) 04014009.
[16] H. Yao, Y. Cao, S. Zhang, B. Wen, A novel energy sink with piecewise linear stiffness, Nonlinear Dynam. 94 (3) (2018) 2265–2275.
[17] S. Benacchio, A. Malher, J. Boisson, C. Touz, Design of a magnetic vibration absorber with tunable stiffnesses, Nonlinear Dynam. 85 (2) (2016) 893–911.
[18] S.L. Feudo, C. Touz, J. Boisson, G. Cumunel, Nonlinear magnetic vibration absorber for passive control of a multistorey structure, J. Sound Vib. 438 (2019) 33–53.
[19] F. Liu, S. Theodossiades, D. McFarland, A. Vakakis, L. Bergman, Tailoring strongly nonlinear negative stiffness, J. Mech. Des. 136 (2) (2014) 024501.
[20] G. Kerschen, K. Worden, A.F. Vakakis, J.-C. Golinval, Past, present and future of nonlinear system identification in structural dynamics, Mech. Syst. Signal Process. 20 (3) (2006) 505–592.
[21] J. Nol, G. Kerschen, No nlinear system identification in structural dynamics: 10 more years of progress, Mech. Syst. Signal Process. 83 (2017) 2–35, https://doi.org/10.1016/j.ymssp.2016.07.020.
[22] B. Vaurigaud, A.T. Savadkoohi, C.-H. Lamarque, Targeted energy transfer with parallel nonlinear energy sinks. part i: design theory and numerical results, Nonlinear Dynam. 66 (4) (2011) 763–780.
[23] K. Dekemele, P. Van Torre, M. Loccufier, Optimization of multi-modal targeted energy transfer performance of nonlinear passive vibration absorbers, in: Proceedings of ISMA 2018: International Conference on Noise and Vibration Engineering, 2018, pp. 4197–4210.
[24] S. Masri, T. Caughey, A nonparametric identification technique for nonlinear dynamic problems, J. Appl. Mech. 46 (2) (1979) 433–447.